J Fluoresc (2009) 19:517–532
DOI 10.1007/s10895-008-0441-z

ORIGINAL PAPER

Control of Two-photon Fluorescence of Common Dyes and Conjugated Dyes

Eric R. Tkaczyk · Alan H. Tkaczyk · Koit Mauring · Jing Yong Ye · James R. Baker Jr. · Theodore B. Norris

Received: 20 July 2008 / Accepted: 3 November 2008 / Published online: 11 December 2008

Abstract We present a comprehensive study of the selective excitation of two-photon fluorescence from various pairs of dyes and dyes in different conjugation states with tailored pulse shapes found with a genetic algorithm (GA). We investigate a number of biologically important dyes, and include dyes conjugated to trastuzumab (Herceptin®) and to a poly(amidoamine) dendrimer. We consider in detail the ability of tailored pulse shaping to discriminate dyes with significant spectral overlap. Our procedure for adaptive pulse shaping includes power-law and chirp-scaling checks to prevent trivial convergences. The GA uses a multiplicative fitness parameter in a graded search method that converges on pulse shapes that not only differentiate two-photon processes, but do so in a high signal regime. We consider the results in terms of not only the absolute maximum ratio of discrimination achieved, but also present the evolutionary course of the GA and compare the improvement to a quantitative measure of the noise level. We also implement a time-domain acousto-optic measurement of two-photon excitation cross-section spectra. The results show that the ability to discriminate dyes is determined almost entirely by their differences in two-photon excitation cross section.

Keywords Two-photon · Coherent control · Pulse shaping · Ultrafast · Dendrimer · Herceptin

E. R. Tkaczyk (✉) · J. Y. Ye · T. B. Norris
Center for Ultrafast Optical Science, EECS Department,
University of Michigan,
2200 Bonisteel Blvd.,
Ann Arbor, MI 48109-2099, USA
e-mail: etkaczyk@umich.edu

E. R. Tkaczyk · J. Y. Ye · J. R. Baker Jr. · T. B. Norris
Michigan Nanotechnology Institute for Medicine
and Biological Sciences, University of Michigan,
Ann Arbor, MI 48109-0648, USA

A. H. Tkaczyk
Department of Biomedical Engineering, University of Michigan,
2200 Bonisteel Blvd.,
Ann Arbor, MI 48109-2099, USA

A. H. Tkaczyk · K. Mauring
Institute of Physics, University of Tartu,
Riia 142,
51014 Tartu, Estonia

Introduction

Multiphoton-induced fluorescence is widely used for biomedical microscopy, *in vivo* sensing, and more recently, flow cytometry [1–8]. Generally, multiple dyes are employed for simultaneous measurements of multiple targets, and these dyes are discriminated by spectral filtering in essentially all high-throughput applications. Laser pulse shaping offers a new avenue of fluorescence discrimination by manipulating the phase and amplitude of an excitation pulse to selectively enhance specific electronic transitions or follow in time the excited state on evolving molecular energy levels. In addition to microscopy, tailored pulse shapes have been successfully applied in spectroscopy [9]. It has already been demonstrated that laser pulse shaping is a successful tool to distinguish fluorescent species [7, 10, 11].

Traditionally, the ability to control fluorescence with shaped pulses has been understood in two ways. The Tannor-Rice control scheme relies on the manipulation of vibrational coherences. The laser pulse is shaped to coherently match the actual trajectory of the excited state wavepacket during its evolution, which is dictated for

example by vibrational relaxation or nuclear motion [12, 13]. A classic example is the pump-dump explanation of increased stimulated emission with negatively chirped laser pulses [14]. The Brumer-Shapiro control scheme, on the other hand, exploits electronic coherences. Energy levels are considered static, and interferences are created between multiple quantum pathways leading to the desired final state. An excellent example is the predictable periodic dependence of the excited state population of cesium on the delay between two optical pulses [15]. In this case, the coherence is between the second pulse and the electrons excited by the first pulse. From a similar vantage point, transform-limited pulses are far from the true optimum to maximize two-photon excitation via a real intermediate level, due to phase differences in the contributions of off-resonant terms [16]. The results we present here, however, are largely explained without consideration of excited wavepacket motion or molecular coherences. Rather, we interpret them in terms of optical intrapulse interferences whose major role is to tune the second-harmonic power spectrum of the exciting pulse to the relevant location on the relative two-photon excitation cross-section spectrum of the discriminated dyes. We thus refrain from the term "coherent control," as coherences in the molecules of interest presumably do not contribute significantly to the selectivity.

One of the primary reasons existing multiphoton applications benefit from pulse shaping is the enhanced specificity to the targeted processes. It has already been shown that simply tuning the fundamental laser excitation wavelength can provide significant information about biological samples in two-photon microscopy [17]. Phase-interferences, however, can achieve far greater specificity [18]. Also, the reduced peak power that generally accompanies shaping of pulses away from the suboptimal transform-limit reduces photobleaching and other undesired multiphoton processes [19].

In the current study, we are particularly interested in the application of coherent control to promising platforms for addressing biological problems with molecular specificity. We investigate the extent to which selective excitation via tailored pulse shaping of two-photon fluorescence from various pairs of dyes and dyes in different conjugation states is possible. We include in the investigation a conjugate to trastuzumab (Herceptin®), which has proven itself as transformative not only in the scientific understanding, but also in the treatment of cancer. Trastuzumab is a humanized monoclonal antibody to the HER2/neu member of the epidermal growth factor receptor, whose overexpression in breast cancer patients is associated with poor prognosis [20, 21]. We consider the effect of dye conjugation to poly(amidoamine) (PAMAM) dendrimers, which are another emergent technology showing great promise in cancer therapy and diagnostics [22, 23]. We also consider tailored pulse shaping to discriminate dyes with significant spectral overlap, which could find practical application in a variety of fluorescence problems.

We first present an overview of our procedure for adaptive pulse shaping, including power-law and chirp-scaling checks to ensure that trivial convergences do not obscure the possibility of true discrimination. Then we describe the details of the genetic algorithm (GA) which, via a multiplicative fitness parameter in a graded search method, converges on pulse shapes that not only differentiate two-photon processes, but do so in a high-signal regime. For interpretation of the results, we are assisted by a time-domain acousto-optic measurement of two-photon excitation cross-section spectra. Before looking to discriminations of dye pairs, we first examine the ability to control fluorescence relative to the simpler same-order process of second harmonic generation (SHG). We consider the results in terms of not only the absolute maximum ratio of discrimination achieved, but also present the evolutionary course of the GA and compare the improvement to a quantitative measure of the noise level.

Materials and methods

Samples

Samples are purchased from Invitrogen Corpororation (Carlsbad, CA) or Excimer Laser Dye Company, as listed in Table 1, with the exception of the dendrimer- and Herceptin- conjugates, which are prepared in house. Fifth generation PAMAM dendrimers are prepared and conjugated to folic acid (FA) and 6-Tamra as described previously [23], to create the G5-6T-FA sample.

The Herceptin-Alexa Fluor 594 conjugate is prepared as follows. 5 mg Herceptin (148 kDa) is dissolved in 3.4 ml phosphate-buffered saline for a 10 μM concentration. To the antibody solution is added 34 μl of 5 mM AF594-SE (*Invitrogen* A20005; AF594 carboxylic acid, succnimidyl ester) in DMSO. The reaction mixture is mixed overnight at room temperature and purified by gel filtration with a Sephadex G25 column (1 cm×30 cm), which is equilibrated with 10 mM phosphate buffer pH 7.0. The fraction that absorbs both at 280 nm and 590 nm is collected and concentrated with a Centricon device (10 K MWCO). An average of 4 or 5 Alexa-Fluor molecules are present per Herceptin in the final mixture.

Experimental setup

Figure 1 shows the experimental setup, which employs a regeneratively amplified Ti:sapphire system (RegA, Coherent,

Table 1 Dyes used in two-photon fluorescent control experiments

Sample	One-photon peak (nm)		Catalog number	Solvent	Concentration (μM)
	Absorption	Emission			
Fluorescein Isothiocyanate (FITC)	495	520	F-143	water	3.33
Calcium Green	506	531	C-3010MP	water	10
6-TAMRA	540	564	C-6123	water	3.33
G5-6T-FA				water	3.33
DiI	549[a]	565[a]	V-22885	DMSO	20
Rhodamine B (Rhodamine 610)	556	578	6102	water	1
TXR-Phalloidin	583	603	T-7471	methanol	~2.2
Texas Red (TXR)	596	615	T-353	methanol	5
Alexa Fluor 594	590	617	A-20004	water	6
Herceptin-AF594				PBS	3
DiD	644[a]	665[a]	V-22887	DMSO	20

All samples were purchased from Invitrogen corporation except rhodamine B, which was purchased from Exciton, and BFP, which was purchased from QBioGene

[a] DiI and DiD absorption and emission are provided for the membrane-bound dyes

Santa Clara, CA). This provides up to 4 μJ, 50 fs pulses at 250 kHz with a center wavelength of 800 nm and 27 nm FWHM bandwidth. To shape the pulses, we use the "Dazzler", an acousto-optic programmable dispersive filter (AOPDF) (Fastlite, Palaiseau, France). Though our laser system is capable of delivering over 1 W of average power, we typically only deliver on the order of 1 mW to 2 mW average power to the sample, which alleviates thermo-optical distortions, amongst others concerns. The diffracted output pulse is modulated by way of an acousto-optic interaction with an RF wave launched into a TeO_2 crystal [24, 25]. In our experiments, a text file is automatically generated by the algorithm, which provides the controlling electronics of the Dazzler the diffracted power, center wavelength, bandwidth, and polynomial phase to fourth order as well as arbitrary phase and amplitude in 20 or more frequency bins within the bandwidth of the laser.

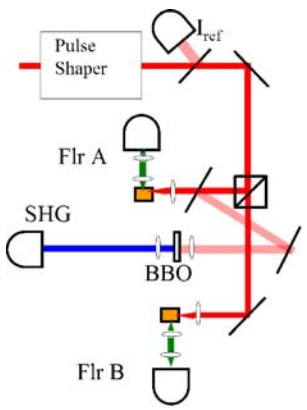

Fig. 1 Experimental Setup. The dye sample is contained in a disposable fluorescence cuvette (Cole Palmer). Incident laser power I_{ref} is measured by a photodiode (R2066, Hamamatsu). After filters to remove all pump laser and exciting 800 nm light, the fluorescence signals FlrA and FlrB are measured in the perpendicular direction by PMTs (H5784-01, Hamamatsu). SHG from the BBO crystal is detected by another PMT (R2066, Hamamatsu). Lenses are depicted as *ovals*

A reference reading of incident power I_{ref} is measured by a photodiode (FFD-100, Perkin-Elmer Optoelectronics, Fremont, CA) from a glass-coverslip beamsplitter. For each two-photon fluorescence signal S, we define an efficiency as the ratio S/I_{ref}. The excitation beam is then divided into two arms with a beamsplitter. The relative power in each arm is controlled with a variable reflective attenuator. Each arm is focused into a cuvette holding the dye sample, to create the fluorescence signal FlrA or FlrB, which is detected through an appropriate bandpass filter (Chroma Technology, Rockingham, VT) by a photomultiplier tube (PMT) (H5784-01, Hamamatsu, Bridgewater, NJ). The FlrA arm additionally has another glass-coverslip beamsplitter to create a third arm of the experiment, where a 500-micron thick beta barium borate (BBO, β-BaB_2O_4) crystal is used for second-harmonic generation. The SHG signal is read through a blue absorptive filter (Chroma Technology, Rockingham, VT) by another PMT (R2066, Hamamatsu, Bridgewater, NJ). A 250 kHz DAQ board (M-series, National Instruments, Austin, TX), synchronized by the Dazzler trigger, is used to read all four signals I_{ref}, FlrA, FlrB, and SHG in parallel as root-mean-square Voltage for 2,500 samples.

Before each experiment, the incident power is scanned to ensure quadratic scaling of the discriminated two-photon processes, as shown in Fig. 2, to avoid artefactual results which might disappear under changing laser power. Wu and Berland have provided insightful calculations and discus-

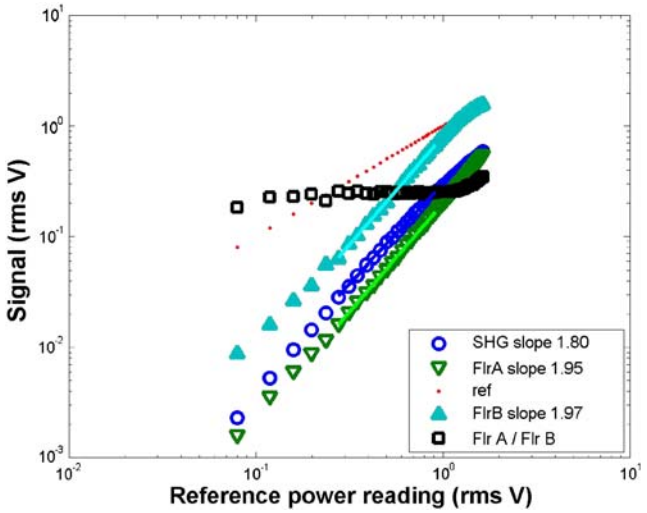

Fig. 2 Power scaling of two-photon signals relative to I_{ref}. *Black squares* show the dependence of the ratio FlrA/FlrB on power. FlrA is signal from 3.33 uM G5-6-Tamra-FA whereas FlrB is signal from 3.33 uM 6-Tamra. *Axes* are in log scale. *Slopes* of a least-squares linear fit through the center of the data are marked in the legend. SHG sub-quadraticity disappeared when an ND filter was placed in front of the detector and therefore results from detector saturation at the higher powers. Perfect quadratic scaling of SHG is seen at lower powers

sion of power scaling in two-photon processes [26]. Notably, subquadratic scaling does not require saturation, and conversely quadratic scaling alone does not preclude saturation effects over part of the pulse. Three possible causes for subquadratic behavior are: saturation of molecular transitions; detector saturation; or scattered excitation light leakage into the detector. Typical diffraction-limited beam fluence at the laser focus during our experiments would be 0.5 mJ/cm^2 (peak intensity on the order of a GW/cm^2 transform-limited), which is too low to saturate the molecular transitions. An independent calibration demonstrating linearity at the measured signal levels rules out detector saturation. Bandpass filters and beam dumps minimize scattered light. Scattered light is not noted to affect the convergence of the algorithm when both signals used in the fitness parameter have the same degree of deviation from quadratic scaling. However trivial convergence of mere pulse stretching can affect results if one dye for example is approaching saturation of the molecular transition while the other is still in the quadratic region. Photobleaching with a recovery time of several seconds is also generally noted for repeated measurements anywhere near the saturation region (Fig. 3). Avoiding photobleaching, which is not necessarily coincident with saturation of molecular transitions, is also important in this case due to the possibility of highly fluorescent photoproducts which will differently affect our measurement of different dyes. Fundamental research into the process of photobleaching still needs to occur for a full understanding of how our measurement process might be affected in this region, and we anticipate great insight from FCS measurements such as those of Widengren and Rigler on rhodamine 6G and FITC [27]. Thus, the power scaling check in each experiment is extremely important.

Even if the incident laser power is unvarying in the course of the adaptive learning algorithm, true control possibilities could still be masked by uninteresting convergences with simple linear chirp (second order polynomial phase) adjustments. Under increasing chirp, two-photon

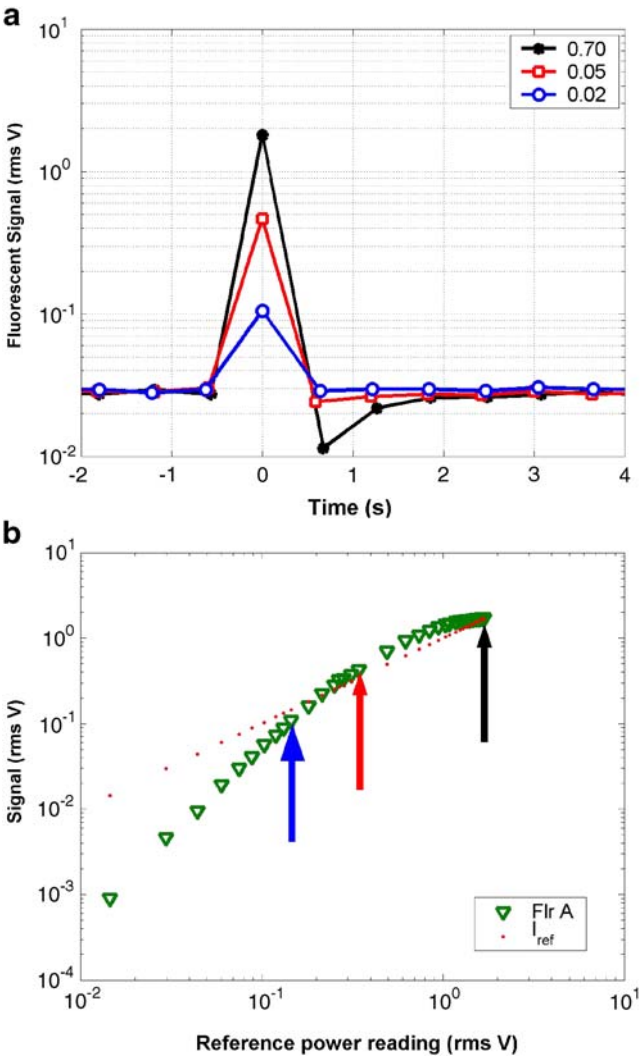

Fig. 3 Dependence of photobleaching on incident power. **a** Net two-photon fluorescent signal from a mixture of DiI and RhodB versus time. At time 0, incident power of 2%, 5%, or 70% of the maximum was sent to the sample (indicated by 0.70, 0.05 and 0.02 on the legend). All other time points had 1% of maximum power incident. **b** Average two-photon fluorescence from mixture versus pulse power (as % of maximum). Applied powers in **a** are marked with *arrows*. The saturation was achieved by permitting higher intensity laser pulses to reach the sample through removal of attenuation

fluorescence in the saturation region for example would not decrease, while the unsaturated SHG signal would decrease with the increased pulse duration [28]. In fact, if the two-photon fluorescence emission has a short enough lifetime to be saturated by peak laser intensity rather than the pulse fluence, the two-photon signal could actually increase with the increased group delay dispersion. Another case in which linear chirp could mask control is when the dispersion in the different materials in the two optical paths is not exactly matched. In this case, the optimal pulse shape would discriminate simply by tuning to compensate dispersion in the appropriate path.

As shown in Fig. 4, when we have carefully set up our experiments, we find little discrimination of two-photon processes by linear chirp adjustment applied by the Dazzler. While it is true that some investigations [14, 29] have shown true coherent control based only on chirp variation, these have generally been at saturating fluences and shown asymmetry with positive versus negative chirp.

Genetic algorithm

The genetic algorithm (GA) relies on two-point crossover and mutation operators inspired by the work of Pearson and colleagues [30]. From an initially random set of pulses, evolutionary improvement follows the fitnesses assigned to the measurements for each pulse, reflecting proximity to the desired outcome. In addition to implementing the GA in an acousto-optic modulator, several modifications we have added include a multiplicative fitness parameter, chromosome circularization, a variable mutation rate, a graded search method, and an unvarying individual in each generation to measure laser stability.

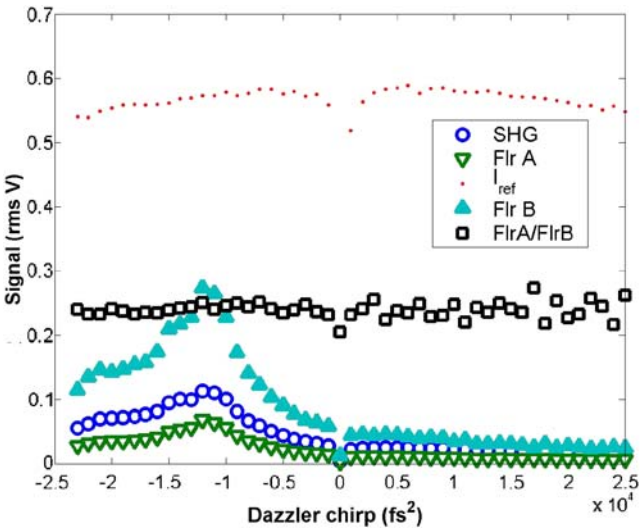

Fig. 4 Lack of discrimination with linear chirp scaling. Scaling of same signals as Fig. 2. with variation in linear chirp (2nd order polynomial phase). Note the drop in diffraction efficiency of the Dazzler when little second-order polynomial phase is applied (zero chirp)

Gene interpretation

Each individual laser pulse in a generation of the GA is defined by a chromosome consisting of 45 or more genes, all of which can vary between 0 and 1. One gene controls the power of the diffracted beam by setting the energy of the acoustic wave, and four genes modify 4th order polynomial phase. Additionally, for each of 20 frequency components, there is an amplitude gene and a phase gene. The number of frequency components for some experiments is increased to as many as 100 to access higher resolution frequency information. The genes are interpreted linearly within prescribed physical limits specified for each experiment, which are generally in line with the constraints of the Dazzler's capabilities. For example, the linear chirp was allowed to vary between −50,000 fs^2 and +50,000 fs^2. The amplitude in a particular frequency bin is simply the direct value of the corresponding amplitude gene. If physical constraint programming is not used, each phase gene is multiplied by 2π to give the programmed phase in that frequency bin.

A more advanced feature that can be employed in the algorithm is physical constraint programming, which limits the interpretation of phase genes to ensure that the shaped pulse falls within an absolute time window [T_{MIN}, T_{MAX}]. These are typically 1 ps and 2 ps to ensure that the trailing edges of the pulse still fall within the 3.6 ps maximal programmable duration within the TeO_2 crystal of the Dazzler. The feature is generally used to obtain the results shown in this paper. Exact implementation is as follows. The derivative of polynomial phase is used to determine the time delay $\tau_{polynomial}$ which a frequency bin would experience in the absence of further phase modulation. This might be less than T_{MIN}, or possibly even a negative number. From this, we set the minimum permissible delay the phase file can add (via its derivative with respect to frequency) as $\tau_{min} = T_{MIN} - \tau_{polynomial}$. Similarly, the maximum permissible delay is set as $\tau_{max} = T_{max} - \tau_{polynomial}$. The range [$\tau_{min}$, τ_{max}] then determines the limits of interpretation for the individual frequency bin genes, which are set such that their derivative adds a delay linearly scaled in this interval. Thus, the combined delay of the frequency bin including both polynomial phase and direct phase will fall in the range [T_{MIN}, T_{MAX}]. One further nuance of our implementation is that genes from 0 to 0.5 are linearly scaled to positive additional delays in the range [max(0, τ_{min}) τ_{max}], and genes from 0.5 to 1 are linearly scaled to negative additional delays in the range [τ_{min} min(τ_{max},0)]. This ensures that the unshaped pulse can

be directly programmed as all ones or zeros. This nuance also requires that, in order to properly exert their effect, the limits [T_{MIN}, T_{MAX}] must be chosen to completely contain the pulse with only polynomial phase modification i.e. $\tau_{MIN} < \tau_{polynomial} < T_{MAX}$ for all frequencies.

Fitness parameters

The results of the experiment depend heavily on the exact form of the fitness parameter assigning the fitness F to each individual in a population. As shown previously [31], SHG and two-photon excited fluorescence of common dyes, both second-order processes, are generally (but not necessarily [16]) maximally efficient with a transform-limited pulse. As an alternative to blind maximization attempts, one can remove the intrinsic nonlinear dependence of the two-photon fluorescent signal A by controlling it relative to the signal B from SHG or another process of the same order. This inspires a ratiometric fitness parameter F = A/B [10, 19]. However, as the two-photon signals can drop significantly for example with changing pulse chirp, we have found that this approach leads to low signal levels with degree of discrimination dictated primarily by the arbitrarily set acceptable low-signal limit [31]. In this regime, true discrimination can be confounded by slight nonlinearities in the detectors or mismatches in optical components of the excitation path. Thus in the current investigation, to optimize a ratio A/B, we employ instead the fitness parameter F = (A-c)(c^{-1}-B), where values of A and B are normalized to the unshaped pulse measurement. We have found that setting c to 0.8 yields the better convergence in our experimental conditions, as opposed to the original implementation of unity for c [32]. If both multiplicands are negative, an infinite negative fitness is given to the pulse. If either multiplicand alone falls below 0, the inverse of the other is taken instead to ensure for example that if B exceeds c^{-1}, further decreases in the optimized signal A towards c result in a decreased (more negative) fitness. This division-free fitness ensures that the optimized signal surpasses or at least is near the signal for an unshaped pulse.

The algorithm considers the array of all raw fitnesses **F** at a population level. To protect the algorithm from domination by a noise-spiked individual, we linearly map the fitnesses so that the median individual is about half as likely to produce offspring as the best individual in the population. In particular, for an individual k with raw fitness F(k), we calculate a scaled fitness $F_{scaled}(k)$ as [30]:

$$F_{scaled}(k) = 2 + [\max(\mathbf{F}) - F(k)]/[\text{median}(\mathbf{F}) - \max(\mathbf{F})] \quad (1)$$

Thus the median individual has a scaled fitness of one whereas the best individual has a scaled fitness of 2. Negative scaled fitnesses are set to 0 and result in non-reproducing individuals.

Evolution, mating and mutation

For the first generation, an initial population of 50 random individuals, with all genes uniformly distributed from 0 to 1, is created and sequentially expressed by the Dazzler for measurement. The top ten individuals, as determined by the fitness parameter, are passed from the old generation on to the next generation unchanged to ensure elitism. The remaining 40 individuals of the new generation are determined by twenty two-point crossover matings of individuals picked randomly from the old generation with probability proportional to their relative scaled fitness. In a two point cross-over of individuals, the two offspring are produced by exchange of all genes of the parents between two random cut points [30]. To prevent location on the chromosome from favoring any genes or groups of genes, we treat the first gene as the adjacent neighbor of the last gene of the chromosome in this process. In other words, the chromosome is circularized by permitting the first cut to occur immediately before the first gene.

In the absence of mutation, there would be no source of genetic variation in our population. Therefore, we permit mutation of each gene of a new offspring by replacing it with probability mp by a completely random value uniformly distributed in the possible range. To keep this process in check, there is a probability 1-mp that the offspring will not be given the chance for mutation at all. For these experiments, we use mp near 0.2 to provide an optimal balance between quickly exploring the vast search space while protecting outstanding gene sets from excessive mutation. One limitation of standard implementations of a genetic algorithm with a low mutation rate is progression to a local minimum once homogeneity takes over the population. Therefore, in our algorithm we vary the mutation rate from one generation to the next. In particular, we scale mp by 1/12 of the inverse of the variance of the population in the preceding generation. As the variance of uniformly distributed random variables is precisely 1/12, mp will be set at 0.2 in the first generation, but will increase to balance the degree of population homogeneity that occurs in the search.

The new population is then sequentially expressed by the Dazzler and measured, and the algorithm thus continues iteratively in pursuit of an optimal pulse shape. Typically the search is divided into the first twenty or thirty generations modifying only the polynomial phase search space, followed by full freedom of the GA to manipulate all genes. We have previously shown that this graded search method converges more quickly for problems like SHG maximization alone [31].

Laser stability evaluation

When we consider the results of multiple GA runs, we would like to know how the extent of improvement compares with possible variation of laser conditions between the experiments. To ensure that maximization and minimization curves for discrimination of an individual dye against SHG or another dye meet with identical experimental conditions, we perform these optimizations in parallel. As many as four different populations are interleaved to evolve simultaneously but independently with different fitness parameters. Further, in each generation, two common additional unvarying individuals are added which do not participate in the evolutionary process. The first of these is a zero power pulse from the Dazzler, thus providing a background offset to subtract from the measurements if necessary, and also reflecting any changes in noise due to electronics or dark-room conditions. The other constant individual encodes an unshaped pulse, which additionally gives a measure of the pulse-to-pulse laser fluctuations. This individual expresses genes only of polynomial phase roughly self-compensating the Dazzler, which is the major dispersive element in the optical system before the sample, and thus provides an approximation of the behavior of the transform-limited pulse.

Pulse characterization

For pulse characterization, we use a commercial SHG-FROG unit [33] (Grenouille 8–50 from SwampOptics, Atlanta, GA) and software (VideoFrog, MesaPhotonics, Santa Fe, NM). To ensure maximum fidelity of the reproduced pulse to that actually measured in the course of the experiment, SHG-FROG is typically performed within 24 h of termination of the experiment.

The 27 nm FWHM bandwidth RegA pulses are slightly beyond the limit of accurate phase recovery with the Grenouille device. However, a spectrometer (S1024DW, Ocean Optics, Dunedin, FL) measure confirmed that the $t=0$ point from the raw Grenouille image corresponds well to the shaped pulse second harmonic spectrum measured from the BBO crystal in our experimental setup. This also verifies that phase-matching does not significantly limit the spectral bandwidth of second-harmonic generation [34] in our BBO crystal, within the 50 nm measurement bandwidth of the Grenouille.

Time-domain two-photon excitation cross-section spectrum measurement

Using the same experimental setup, we implement a time-domain measurement of the two-photon excitation cross-section spectrum of dyes in the region of interest. This is performed analogously to the description by Ogilvie and colleagues [35]. In our case, a virtual Michelson interferometer is programmed into the Dazzler. A delay of t_0 between pulses is achieved with simple multiplication by a cosine amplitude mask $\cos(\omega t_0/2)$ in the frequency domain for 150 intervals in an 80 nm bandwidth. We use binary coding of the phase file to be at zero or pi corresponding to the sign of the cos function. Absolute and linear phase are physically irrelevant because the information is actually contained in the interarrival period of the two pulses [36]. After a Fourier transform of the data, the two-photon excitation cross-section is extracted as the divisor of the fluorescent signal by the second-harmonic signal in the region of the $2\omega_0$ component. For detailed mathematical proof of this, the reader is referred to the article by Naganuma et al. [37] or Trebino's discussion [38]. It is noted that our measurement only obtains the relative spectrum of the two-photon excitation cross-section. Readers interested in absolute measurements of two-photon cross-sections are referred to the technique from the group of Rebane [39].

In practice, due to the non-transform limited nature of the unshaped pulse, superior results are obtained when the GA is first run to maximize SHG efficiency to ensure an optimal transform-limited pulse, as shown in Fig. 5. This phase and amplitude is then used as the fundamental pulse for programmed duplication in the time-domain measurement.

Representative data concurrently measuring two dyes in parallel is shown in Fig. 6 in both time and frequency domain.

Results and discussion

The main results of our study are given in Table 2. The objective is to determine the extent to which pulse shaping

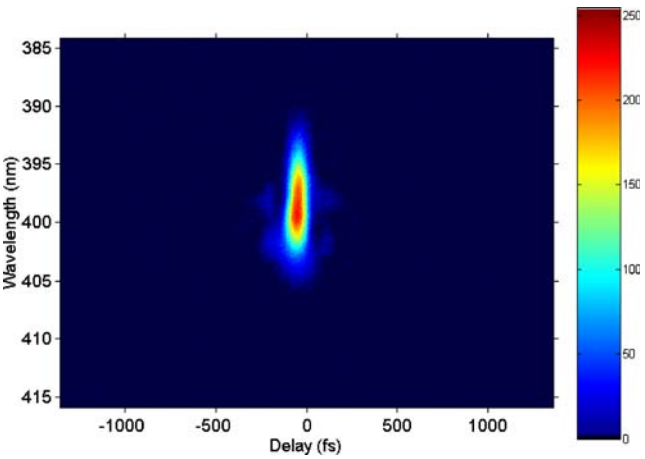

Fig. 5 Optimal pulse from a GA run to maximize SHG/I_{ref}, as measured by SHG-FROG

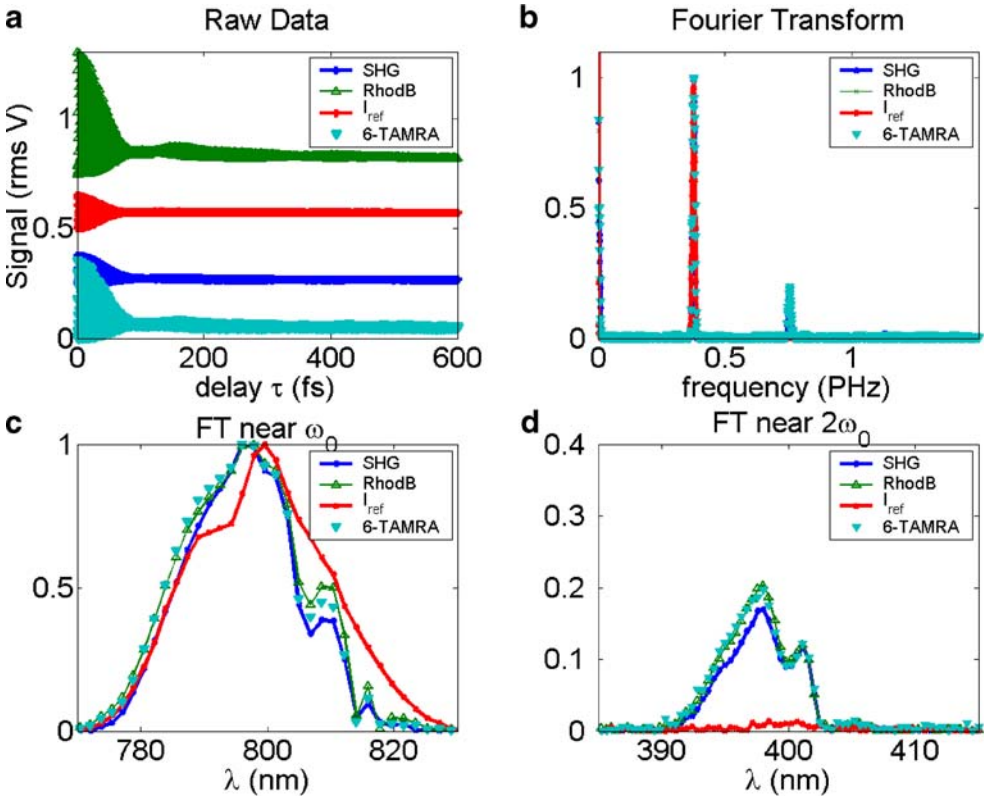

Fig. 6 Time domain measurement of two-photon excitation cross sections of rhodamine B and 6-TAMRA. **a** Absolute signal strength versus programmed delay between the replicated pulses. **b** Fourier transform view. The fundamental frequency of our 800 nm excitation is 0.37 PHz. **c** Detail of peak at the fundamental optical carrier frequency. **d** Detail of second harmonic peak of the signals

may be used to enable discrimination of biologically important dyes with overlapping spectra in two-photon fluorescence. More interestingly, we wish to determine whether an unbound dye may be discriminated from the same dye bound to a specific molecular conjugate. One potential practical application of tailored pulse shaping might be the assessment of delivery success of targeted compounds like a G5 dendrimer to specific cell types or cells in a tissue. If multiple fluorescent molecules are used, traditional methods may be frustrated by spectral overlap

Table 2 Summary of experimental results for discrimination of two-photon processes

Signal A	Signal B	Maximum A/B	Minimum A/B	Maximum discrimination	Relative increase	Noise A	Noise B
BFP	SHG	1.42	0.44	3.27	2.11	0.029	0.013
RhodB	SHG	1.43	0.58	2.48	1.93	0.014	0.017
Her-AF594	SHG	1.17	0.63	1.87	1.36	0.034	0.034
TXR	SHG	1.22	0.64	1.89	1.28	0.021	0.041
G5-6T-FA	SHG	1.10	0.80	1.38	1.18	0.023	0.015
DiI	FITC	1.90	0.67	2.82	1.94	0.037	0.022
BFP	DiI	1.21	0.41	2.98	1.79	0.024	0.044
DiI	RhodB	1.76	0.62	2.83	1.57	0.047	0.034
DiI	DiD	1.61	0.70	2.31	1.55	0.031	0.029
DiI	RhodB	1.28	0.62	2.08	1.10	0.027	0.027
Ca Green	Rhod B	1.23	0.81	1.51	1.07	0.050	0.020
TXR	AF594	1.14	0.91	1.24	1.06	0.041	0.042
Rhod B	6-TAMRA	1.12	0.90	1.25	1.02	0.029	0.028
TXR-phal	TX Red	1.23	0.85	1.45	1.13	0.035	0.016
Her-AF594	AF594	1.14	0.87	1.31	1.07	0.063	0.026
G5-6T-FA	6-TAMRA	1.10	0.90	1.22	1.06	0.048	0.035

The maximum discrimination is the ratio A/B for the maximizing pulse divided by the ratio for the minimizing pulse. The relative increase is the maximum discrimination divided by the maximum discrimination achieved in the first 20 generations of the GA, during polynomial-only modification. "Noise" is the standard deviations of the measurement of the unshaped pulse, normalized to the mean measurement

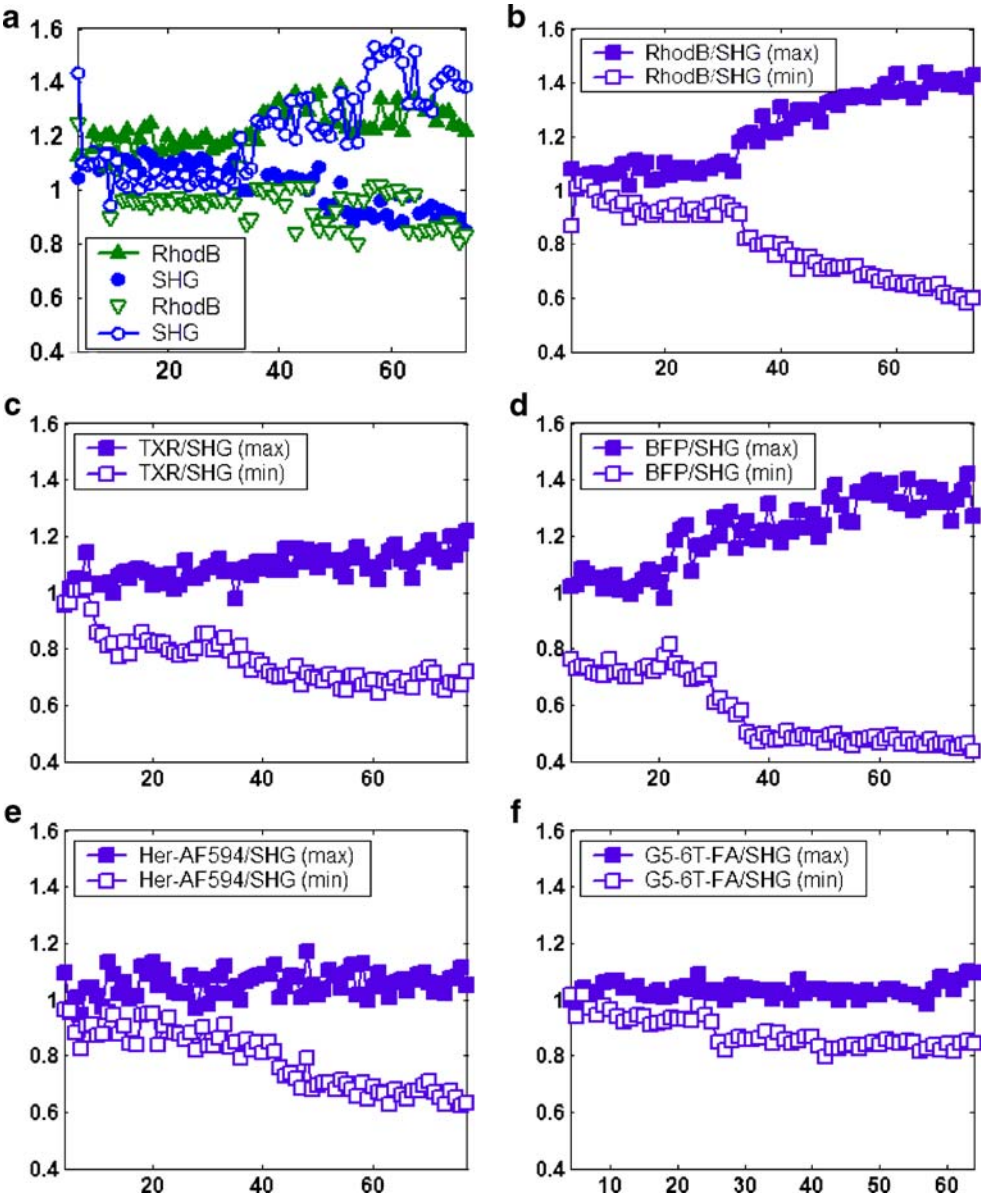

Fig. 7 Control of the ratio of two-photon fluorescence to SHG versus generation of GA for various dyes. Measurements of each generation's best individuals for maximization of FlrA/SHG are shown with closed markers, whereas results of the parallel minimization experiment are shown with open markers (for example, *filled circles* are the SHG measurements of the best individual of the generation for the parallel maximization experiment, whereas *hollow circles* represent SHG measurements of the best individual of the generation for the minimization experiment). All measurements are shown normalized to the corresponding measurement for the unshaped pulse. **a** rhodamine B/SHG. *Blue circles* show SHG efficiency (SHG/I_{ref}). *Green triangles* show rhodamine B fluorescence efficiency. **b** Ratio of rhodamine B fluorescence to SHG for the same experiment pair. **c** control of Texas Red/SHG ratio **d** BFP **e** Herceptin-conjugated AlexaFluor 594 **f** Fifth-generation-dendrimer with conjugated 6-TAMRA and folic acid

between the markers or with an autofluorescent background. Further, conjugation state usually does not affect one-photon spectra, and therefore differentiating specific uptake of targeted molecules conjugated to a reporter dye from nonspecific uptake of these molecules is not generally possible by simple spectral filtering. We find in our investigation that shaped pulses can enhance or suppress the fluorescence of many common reporter dyes relative to SHG, which could be a significant source of fluorescent background for example in a collagen-dense tissue. We also control the relative fluorescence of dye pairs with variable success, proving that our tailored pulse shapes are sometimes, but not always, a useful discrimination technique. Further, the degree of discrimination achieved with shaped two-photon excitation pulses is not correlated with one-photon spectral distinction or overlap. Rather, the predominant mechanism of discrimination is found to be tuning of the second-harmonic spectrum of the excitation laser pulse to the relative maxima and minima of the two-photon excitation cross-sections of the target dyes. These cross-sections do not change within the bandwidth of our measurement with conjugation of AlexaFluor 594 to Herceptin or 6-TAMRA to a dendrimer, and therefore we are unable to distinguish these conjugation states in our experiments. To change the two-photon excitation cross-section of a fluorophore, we believe that a strong electronic interaction must occur. An example of a conjugation sufficient for this result is Texas Red to phalloidin, which our method is able to successfully detect.

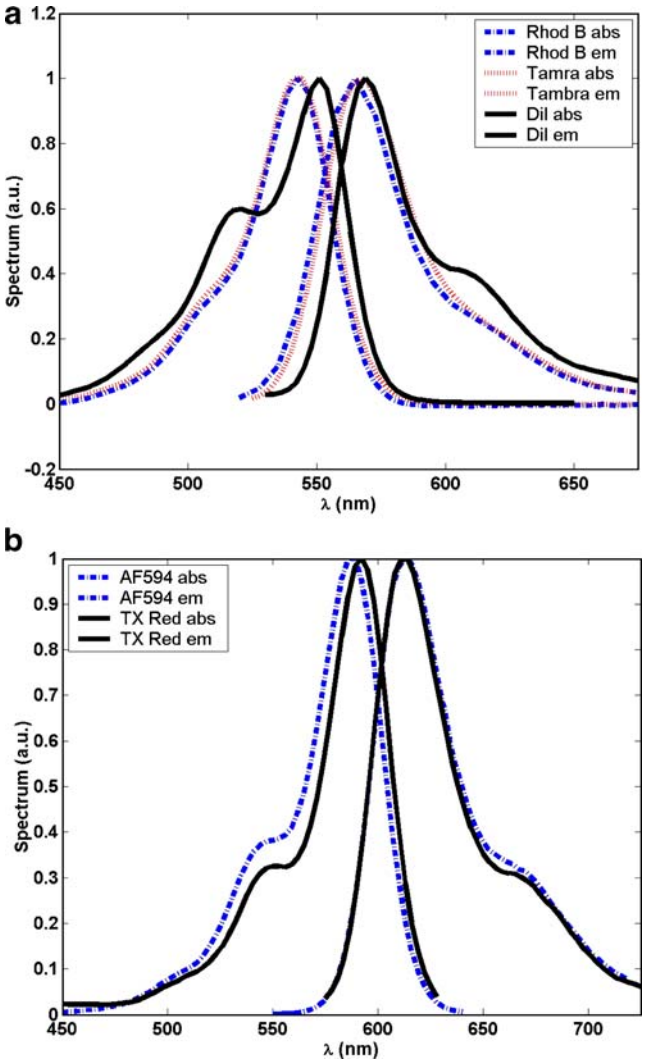

Fig. 8 Overlapping absorption and emission spectra of **a** rhodamine B, 6-TAMRA, and DiI and **b** Alexa Fluor 594 and Texas Red. [50, 51]

Compiled results are summarized in Table 2, showing the ratio of two-photon signal achieved for the maximizing and minimizing pulses. It is important not only to look at the absolute ratio of control achieved, but also details of the GA run that are also included in Table 2. For example, if the best degree of control is very high but little or no improvement occurs after the generations of polynomial-only search, this may indicate noise of excessive laser pulse-to-pulse variation or other instabilities. The degree of fluctuations in measurements of the unshaped pulse between generations reflects the degree of laser stability, and it is quanitified as the standard deviation of the unshaped laser pulse, normalized to the mean. Generally this was less than 5% per channel. An example with greater fluctuations is the discrimination experiment with Herceptin-conjugated AlexaFluor 594. That particular experiment had approximately 9% total noise from both channels, but only 7% improvement after the polynomial search portion of the search. By comparison, the BFP to SHG discrimination had 111% increase in control after the end of polynomial search, with only 4.2% total noise between the two channels (Table 2).

Control of two-photon fluorescence relative to SHG

For all dyes, tailored pulses met with varying degrees of success in controlling the ratio of two-photon fluorescence to SHG (Fig. 7). At the same time as controlling this ratio, there is no drop in the maximized signal relative to the unshaped pulse. An example is the maximization of two-photon fluorescence of rhodamine B, whose efficiency is marked with closed green triangles of Fig. 7a, at the expense of SHG (closed blue circles). These measurements are plotted normalized to the unshaped pulse, and clearly the maximized signal's normalized efficiency never drops below one. This is in distinction from previous results, where the algorithm with a ratiometric fitness parameter generally converged to the minimum permissible signal level [31]. The consistent high signal levels found with a multiplicative fitness parameter are a great advantage if the pulses are to subsequently be applied in signal-limited situations.

In some cases, both maximization and minimization experiments converge on significant discrimination, whereby the ratio of fluorescence signal to SHG can be both increased and decreased significantly from unity (e.g. rhodamine B Fig. 7b or BFP Fig. 7d). More commonly, the fluorescence can be only modestly improved relative to SHG, but it can on the other hand be significantly decreased relative to SHG. This is manifested as a greater departure from unity during the maximization experiment than during the minimization experiments performed in parallel. For example, the folic acid (FA)-G5-dendrimer-conjugated 6-TAMRA fluorescence can be decreased 20% relative to SHG, but improved by under 10% (Fig. 7f).

Discriminability is not necessarily correlated with one-photon spectral distinction

Many of the dyes we have controlled have significant overlap in one-photon spectra (Fig. 8).

Figure 9 shows convergence of the GA to discriminate various dye pairs with tailored pulses. We discover that the degree of control is not predictable by that achieved relative to SHG for each individual dye. For example, both 6-TAMRA (conjugated to G5-FA) and rhodamine B had significant control relative to SHG (Fig. 7b and f), yet discrimination of rhodamine B from 6-TAMRA met with limited success (Fig. 9c). The difficulty in using one-photon excitation or emission to differentiate the pair of rhodamine B and 6-TAMRA (Fig. 8a) is thus not significantly ameliorated by the application of tailored two-photon

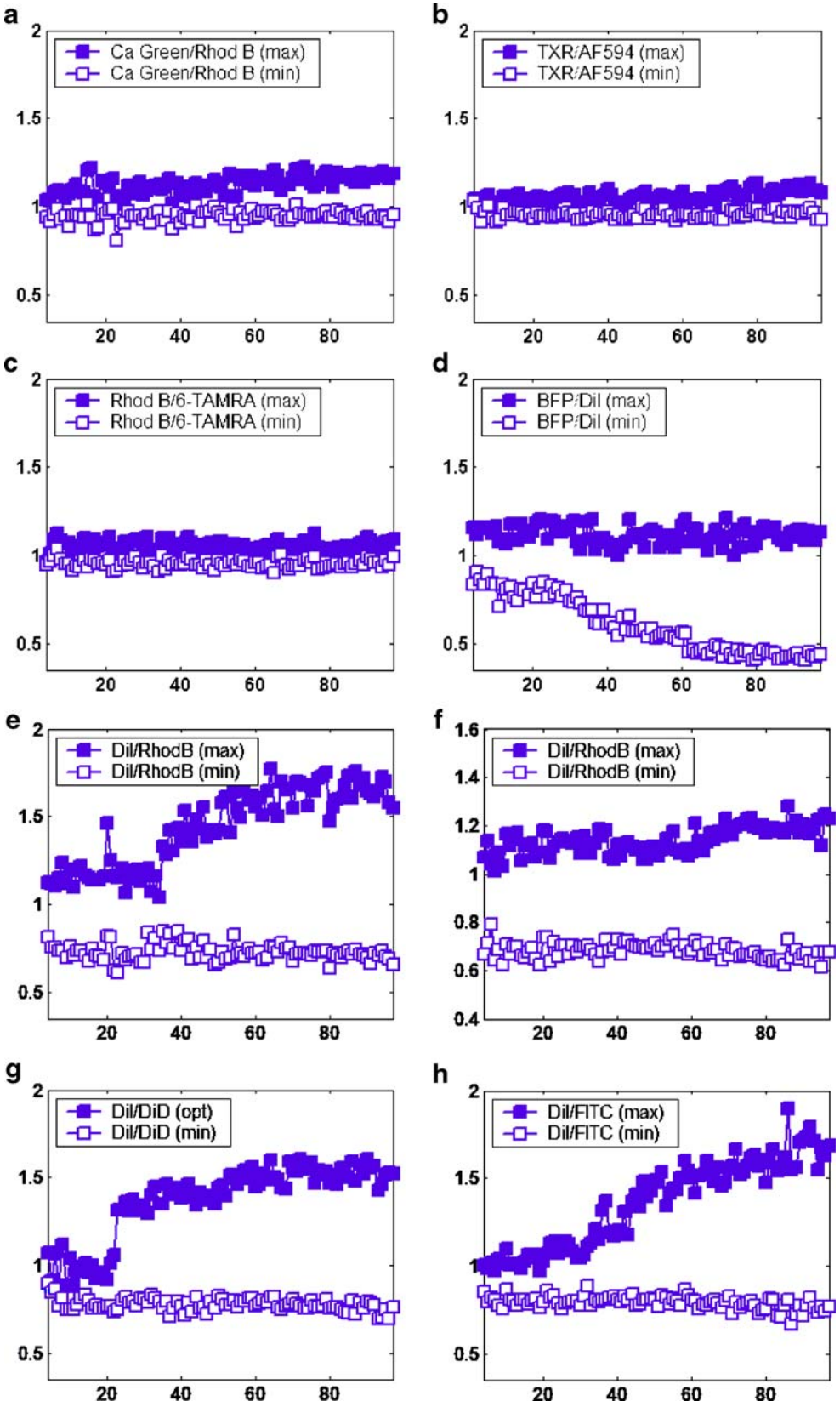

Fig. 9 Control of the ratio of two-photon fluorescence from various dye pairs versus generation of GA. *Closed squares* show maximization of the ratio, and *open squares* mark the parallel experiment minimizing the same ratio (optimizing the inverse ratio)

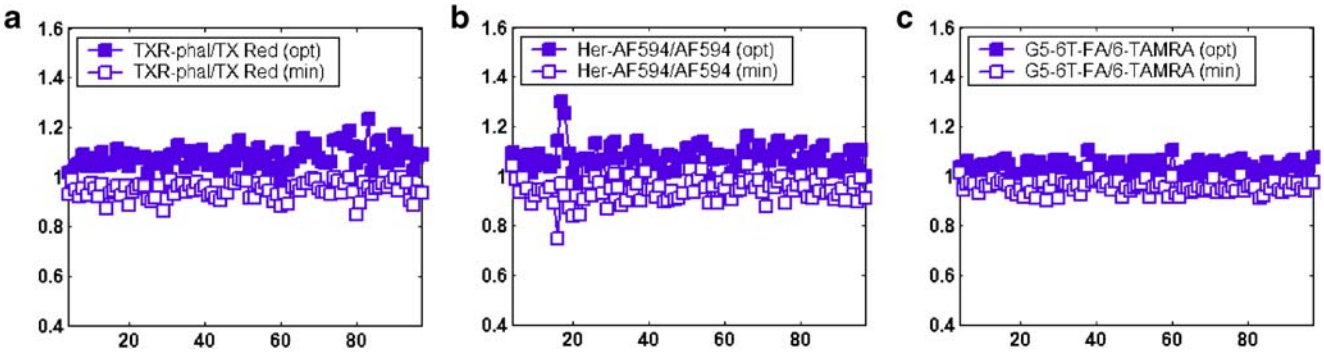

Fig. 10 Control of the ratio of two-photon fluorescence from conjugated to free dye versus generation of GA. *Closed squares* show maximization of the ratio, and *open squares* mark the parallel experiment minimizing the same ratio (optimizing the inverse ratio)

excitation pulses. This is also the case for the one-photon spectrally indistinguishable pair Texas Red and AlexaFluor 594 (Figs. 8b, 9b). On the other hand, some dyes which are easily discriminated by means of their one-photon spectra, for example DiI and FITC, are quite amenable to differentiation by our GA (Fig. 9h).

Identical one-photon spectra do not preclude two-photon distinction via pulse shaping, since two-photon processes obey different quantum selection rules [40–42]. For example, rhodamine B and DiI are distinguished by our GA to a significant extent (Fig. 9e) despite almost complete overlap of both one-photon excitation and emission spectra, though the exact amount of discrimination found by the GA varies (Fig. 9f). We are even able to use this capability to quantify the concentration of DiI and rhodamine B in a mixture of the two dyes [43].

Finally, dyes with different one-photon spectra are not necessarily more distinguishable with our method than the overlapping dyes. For example, rhodamine B and calcium green have distinguishable one-photon spectra, but are more poorly differentiated (Fig. 9a) by our shaped pulses than the rhodamine B and DiI pair.

Determination of the conjugation states of dyes

Figure 10 summarizes attempts to discriminate two-photon fluorescence of free from conjugated dyes. One arm of these experiments measures the dye's fluorescence in free solution while the other arm measures the fluorescence of the same dye chemically conjugated to another compound. For both the dendrimer and Herceptin conjugates, the degree of improvement in control after polynomial phase search by the GA is smaller than the combined error of the two signals (Table 2). However, for the F-actin-binding protein phalloidin, the differentiation of free versus bound Alexa Fluor 594 dye is significant by this measure.

In general, we believe that the conjugation state of a dye can only be determined with pulse shaping if there is a reasonably strong electronic interaction between the excited state orbital of the dye and the molecular orbitals of the conjugate molecule. Good evidence for such an interaction is a significant change of two-photon excitation cross-section spectrum for the dye upon binding, which has previously been shown to occur when Texas Red is conjugated to phalloidin [44].

Mechanism of fluorescence control

A common practice in the investigation of tailored pulse shaping is to look at the correlation of the outcome of the experiment with SHG (a surrogate for pulse compression), with the assumption that presence or absence of good correlation is a measure of the complexity of the control problem. For example, a simple problem like multiphoton ionization of a molecule might translate into maximizing the peak pulse energy. As the problem of SHG maximization also maps to the same underlying mechanism, a strong correlation is seen between multiphoton ionization and SHG in an adaptive search to maximize either [45, 46]. Figure 11 shows this analysis for the DiI/FITC discrimination. No noticeable correlation is evident between the degree of discrimination of the pulse shapes and the SHG efficiency. This demonstrates that the discrimination mechanism does not map directly onto the simple problem of maximizing peak laser intensity. Despite the lack of correlation of the discrimination problem with SHG, second harmonic spectral tuning will be seen to provide an adequate explanation for the control.

Detailed information for optimal discriminating pulses is revealed in a time-frequency picture. Figure 12 shows the SHG-FROG traces in the case of rhodamine B and SHG. The complementary nature of the pulses for maximization and minimization is consistent with our previous observations [31]. Often, part of the exciting laser field is broken down into a series of pulses, characteristic of control of an excited state wavepacket's motion in coherence with vibrational energy level changes [47]. However, most of the pulse energy is nevertheless confined to short delay

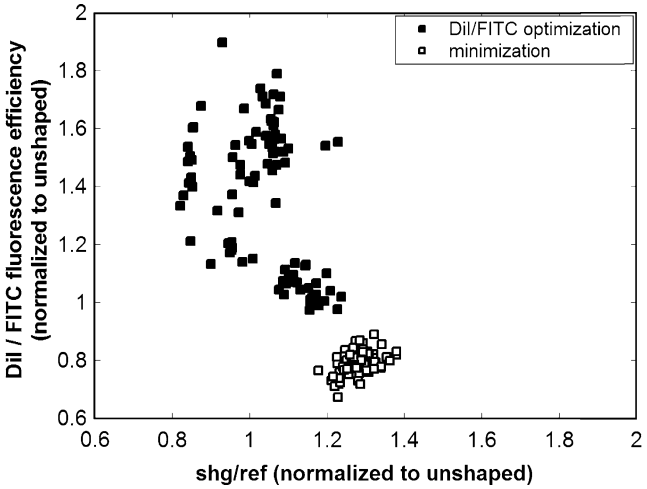

Fig. 11 Correlation analysis of DiI vs FITC discrimination experiment from Fig. 9h. DiI/FITC fluorescence efficiency ratio of the best individual for each of 100 generations is plotted against the corresponding SHG efficiency (SHG/I_{ref}). *Closed squares* show the maximization of the ratio, and *open squares* mark the parallel minimization experiment

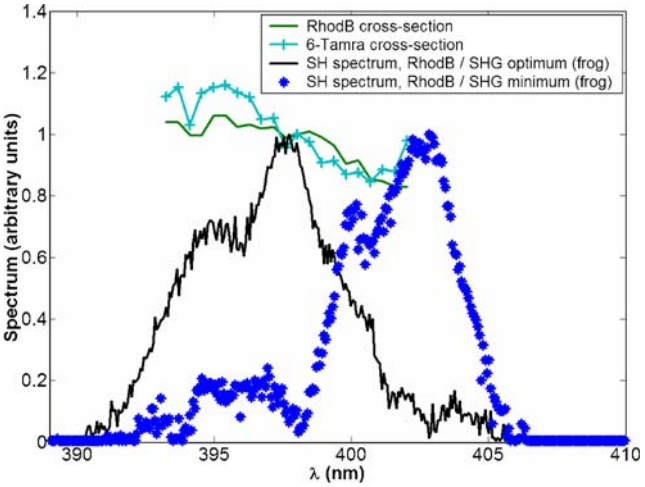

Fig. 13 Tuning of pulse second harmonic spectrum to optimal position of two-photon excitation cross-section spectrum. Time domain measured two-photon excitation cross-sections of rhodamine B (*green line*) and 6-TAMRA (*cyan line* with plusses). Also shown are the second harmonic spectrum of optimal pulses for maximization (*black line*) or minimization (*blue asterixes*) of rhodamine B fluorescence/SHG ratio, determined from FROG traces in Fig. 12

times. Thus, a second order perturbation analysis gives significant insight into the underlying mechanism of discrimination [45]. The essential parameters are the second harmonic spectrum $S_2(\omega)$ of the pulse and the two-photon excitation cross-section $\sigma^{(2)}(\omega)$ of the dye. The spectrum at zero time delay on the SHG-FROG trace is in fact $S_2(\omega)$. Whereas the SHG signal is the total integral of $S_2(\omega)$, the fluorescent signal is the integral of the product of S_2 and $\sigma^{(2)}$. Thus, the pulse optimizing the fluorescence to SHG ratio is achieved by tuning $S_2(\omega)$ to peak in the region where $\sigma^{(2)}(\omega)$ peaks as well, whereas minimization is achieved by tuning $S_2(\omega)$ to peak away from this region. Figure 13 reveals this tuning of $S_2(\omega)$ (extracted from the traces of Fig. 12) relative to the rhodamine B cross-section spectrum we measured in the time-domain. Also shown is the spectrum of $\sigma^{(2)}$ for 6-TAMRA, which was simultaneously measured from the other arm of the setup. Noting the similar shape of these cross-sections, it becomes clear why our GA was unable to distinguish these two dyes despite their individual fluorescence controllability relative to SHG (Table 2). Thus, our acousto-optic time-domain cross-section spectrum measurement yields a prediction of the success or failure of our method to distinguish any attempted dye pair.

Several ratios of cross-sections we measured are plotted in Fig. 14. Within the second harmonic spectral bandwidth of the laser pulses, we measured strikingly flat curves for the pair of Texas Red vs. Alexa Fluor 594 (Fig. 14a). The G5-FA-conjugated vs. free 6-TAMRA pair also seems quite flat (Fig. 14b), though the measurement suffers greater noise. As our experiment operates in the same spectral range, it is not able to discriminate the two dyes by a simple tuning of the second-harmonic spectrum $S_2(\omega)$. The under 25% total control (Table 2) in differentiating these pairs is thus the

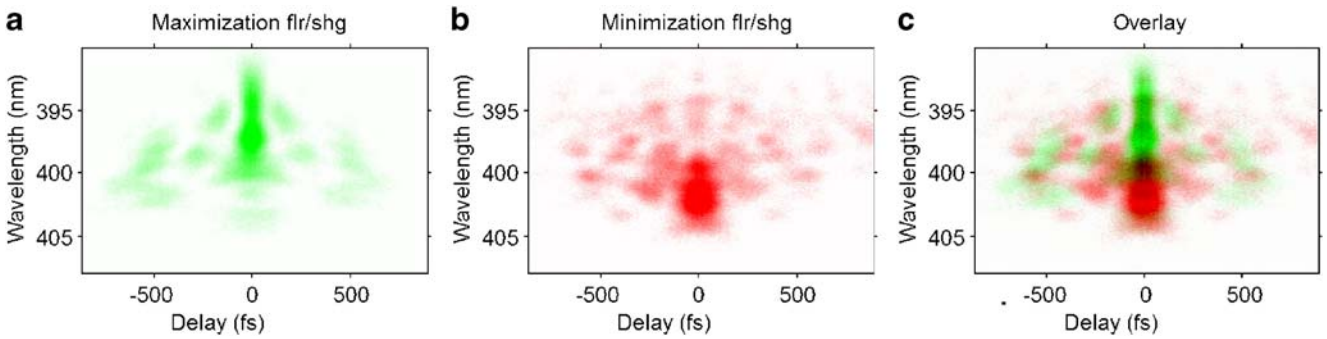

Fig. 12 Optimal pulses measured by SHG-FROG for **a** maximization and **b** minimization of ratio of rhodamine B two-photon fluorescence to SHG from the experiment (shown in Fig. 7a,b), and **c** overlay

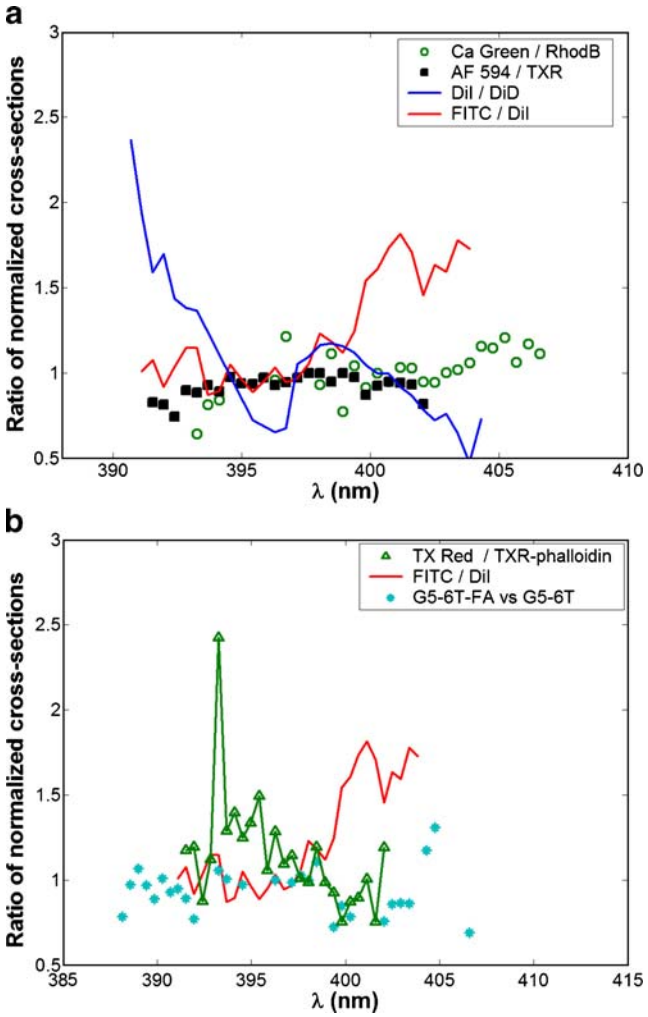

Fig. 14 Relative two-photon excitation cross-sections of several dye pairs, as measured acousto-optically in the time-domain. *Plotted* is the directly measured ratio of two-photon excitation cross-section of the first dye to that of the second dye at each wavelength

result of a fundamental physical limitation. The direction of tuning of $S_2(\omega)$ we measured was always consistent with the relative cross-section in successful discriminations.

Conclusion

We have used tailored femtosecond pulses to control two-photon fluorescence of several common dyes relative to second harmonic generation, which fundamentally has the same nonlinear dependence. We have further studied the ability of our evolutionary learning algorithm to find pulses which selectively enhance or suppress two-photon fluorescence of one dye or dye-conjugate relative to another. While the controllability of individual dyes against SHG does not predict the success of the latter trials, we find that the ratio of two-photon excitation cross-section spectra for the dyes is always consistent with the tuning of the second harmonic spectrum of the excitation pulses. Therefore, we conclude that photon-photon interferences play the major role in discrimination. These interferences are best accessed with arbitrary phase modulation beyond the fourth order polynomial phase, and therefore typical GA runs experience the most significant improvement after the period of restriction to polynomial modulation is passed in our graded search algorithm. On the other hand, we have also previously shown that limiting the size of the search space during arbitrary phase and amplitude modulation is crucial to optimal GA performance [52]. Interestingly, the ability to distinguish dye pairs was uncorrelated with the utility of one-photon spectra to discriminate the dyes, due to the fundamentally different processes responsible for one- vs. two-photon excitation.

Systematic errors from mismatches in different arms of the experiment including dispersion, saturation, or other causes of subquadratic scaling can be removed by examining the improvement of the GA after the graded search has progressed to full phase modulation. Further comparing the degree of enhancement to laser instabilities reflected in repeated measurements of the unshaped pulses lends insight into the true extent of discrimination achieved in our experiments.

Considering the relative improvement compared to the noise in the measurements, the evolutionary search was unable to recognize Herceptin or PAMAM dendrimer-conjugation in our experiments. This may not be surprising, considering the lack of change upon conjugation of two-photon excitation spectra we measured with the acousto-optic time domain method in the bandwidth of our exciting laser pulse. In the event of a strong electronic coupling to the dye molecule upon conjugation, which would be reflected in a change of two-photon excitation spectrum, our method is more likely to succeed. This is evidenced in the case of discrimination of phalloidin-bound from free Texas Red dye. Another example of a strong interaction with a dye would be an antibody binding to the dye. In the future we hope to exploit this to develop molecular assays based on detection of precisely these binding events.

There are several aspects of the work presented here which may prove valuable in the eventual practical application. Firstly, the multiplicative fitness parameter of our genetic algorithm is able achieve significant discrimination without a drop in signal of the favored fluorophore, which is very advantageous for signal-to-noise ratio limited measurement techniques. Secondly, the lack of positive or negative correlation of one-photon differentiation with two-photon tailored pulse distinguishability will help us to validate systems relying on tailored pulse shaping with spectrally distinct dyes, and then subsequently apply it to differentiate dyes which are otherwise indistinguishable, for example rhodamine B and DiI. In fact, we have shown in

another series of experiments that unknown mixtures of this dye pair can be quantified through the pulse shapes found by our genetic algorithm [43]. Finally, the exciting pulse phase can be rapidly modulated in an acousto-optic programmable dispersive filter like the Dazzler for high throughput applications. In these cases, the reconfiguration time for one or more laser sources and emission filters traditionally used for discrimination would be prohibitive. Even compared to the standard liquid crystal pulse shaping for selective excitation, the acousto-optic method enables reduction of typical switching times of tens of milliseconds [48, 49] into the submillisecond regime [7].

Acknowledgements This project was supported in full or in part by the cooperative award ESEI-2900-TR-07 from the Estonian Science Foundation and the United States Civilian Research and Development Foundation. During this investigation, ET was supported initially by the University of Michigan MD/PhD program and then by an NSF Graduate Research Fellowship. The authors are indebted to Gary Luker, Andrzej Myc, and Thommey Thomas for samples. A visit by Daniel Kaplan was instrumental in proper operation of the Dazzler and also to develop physical constraint programming in the GA. We would also like to express our gratitude to Daniel Kane and Rick Trebino for numerous stimulating phone conversations about the FROG technique.

References

1. Zipfel WR, Williams RM, Webb WW (2003) Nonlinear magic: multiphoton microscopy in the biosciences. Nat Biotechnol 21:1369–1377 doi:10.1038/nbt899
2. König K (2000) Multiphoton microscopy in life sciences. J Microsc 200:83–104 doi:10.1046/j.1365-2818.2000.00738.x
3. Squirrell JM, Wokosin DL, White JG, Bavister BD (1999) Long-term two-photon fluorescence imaging of mammalian embryos without compromising viability. Nat Biotechnol 17:763–767 doi:10.1038/11698
4. Zhong C, Ye J, Myc A, Thomas T, Bielinska A Jr, Norris T (2005) Two-photon flow cytometry. In: Periasamy A, So P (eds) SPIE 5700:78–89
5. Tkaczyk ER, Zhong CF, Ye JY, Myc A, Thomas T, Cao Z, Duran-Struuck R, Luker KE, Luker GD, Norris TB, Baker JR Jr (2008) In vivo monitoring of multiple circulating cell populations using two-photon flow cytometry. Opt Commun 281:888–894 doi:10.1016/j.optcom.2007.10.106
6. Tkaczyk ER, Tkaczyk AH, Katnik S, Ye JY, Luker KE, Luker GD, Myc A, Baker JR, Norris TB (2008) Extended cavity laser enhanced two-photon flow cytometry. J Biomed Opt 13 (4):041319
7. Ogilvie JP, Débarre D, Solinas X, Martin JL, Beaurepaire E, Joffre M (2006) Use of coherent control for selective two-photon fluorescence microscopy in live organisms. Opt Express 14:759–766 doi:10.1364/OPEX.14.000759
8. Zhong CF, Tkaczyk ER, Thomas T, Ye JY, Myc A, Bielinska AU, Cao Z, Majoros I, Keszler B, Baker JR, Norris TB (2008) Quantitative two-photon flow cytometry—in vitro and in vivo. Journal of biomedical optics 13(3):034008-1-034008-19
9. Dudovich N, Oron D, Silberberg Y (2002) Single-pulse coherently controlled nonlinear Raman spectroscopy and microscopy. Nature 418:512–514 doi:10.1038/nature00933
10. Brixner T, Damrauer NH, Niklaus P, Gerber G (2001) Photoselective adaptive femtosecond quantum control in the liquid phase. Nature 414:57–60 doi:10.1038/35102037
11. Lozovoy V, Pastirk I, Walowicz K, Dantus M (2003) Multiphoton intrapulse interference II. Control of two- and three-photon laser induced fluorescence with shaped pulses. J Chem Phys 118:3187–3196 doi:10.1063/1.1531620
12. Cao J, Che J, Wilson KR (1998) Intrapulse dynamical effects in multiphoton processes: theoretical analysis. J Phys Chem A 102:4284–4290 doi:10.1021/jp973097t
13. Tannor DJ, Kosloff R, Rice SA (1986) Coherent pulse sequence induced control of selectivity of reactions: exact quantum mechanical calculations. J Chem Phys 85:5805–5820 doi:10.1063/1.451542
14. Bardeen CJ, Yakovlev VV, Squier JA, Wilson KR (1998) Quantum control of population transfer in green fluorescent protein by using chirped femtosecond pulses. J Am Chem Soc 120:13023–13027 doi:10.1021/ja9824627
15. Blanchet Vr, Nicole Cl, Bouchene M-A, Girard B (1997) Temporal coherent control in two-photon transitions: from optical interferences to quantum interferences. Phys Rev Lett 78:2716–2719 doi:10.1103/PhysRevLett.78.2716
16. Dudovich N, Dayan B, Gallagher Faeder SM, Silberberg Y (2001) Transform-limited pulses are not optimal for resonant multiphoton transitions. Phys Rev Lett 86:47–50 doi:10.1103/PhysRevLett.86.47
17. Laiho L, Pelet S, Hancewicz T, Kaplan P, So P (2005) Two-photon 3-D mapping of ex vivo human skin endogenous fluorescence species based on fluorescence emission spectra. Journal of Biomedical Optics 10(2): 024016-1-024016-10
18. Lozovoy V, Dantus M (2005) Systematic control of nonlinear optical processes using optimally shaped femtosecond pulses. ChemPhysChem 6:1970–2000 doi:10.1002/cphc.200400342
19. Kawano H, Nabekawa Y, Suda A, Oishi Y, Mizuno H, Miyawaki A, Midorikawa K (2003) Attenuation of photobleaching in two-photon excitation fluorescence from green fluorescent protein with shaped excitation pulses. Biochem Biophys Res Commun 311:592–596 doi:10.1016/j.bbrc.2003.09.236
20. Yarden Y (2001) The EGFR family and its ligands in human cancer: signalling mechanisms and therapeutic opportunities. Eur J Cancer 37:3–8 doi:10.1016/S0959-8049(01)00230-1
21. Mendelsohn J, Baselga J (2003) Status of epidermal growth factor receptor antagonists in the biology and treatment of cancer. J Clin Oncol 21:2787–2799 doi:10.1200/JCO.2003.01.504
22. Majoros IJ, Thomas TP, Mehta CB, Baker JR (2005) Poly(amido-amine) dendrimer-based multifunctional engineered nanodevice for cancer therapy. J Med Chem 48:5892–5899 doi:10.1021/jm0401863
23. Thomas T, Ye JY, Chang Y-C, Kotlyar A, Cao Z, Majoros I, Norris TB, Baker JR (2008) Investigation of tumor cell targeting of a dendrimer nanoparticle using a double-clad optical fiber probe. J Biomed Opt 13:014024 doi:10.1117/1.2870105
24. Verluise F, Laude V, Huignard JP, Tournois P, Migus A (2000) Arbitrary dispersion control of ultrashort optical pulses with acoustic waves. J Opt Soc Am B 17:138–145 doi:10.1364/JOSAB.17.000138
25. Kaplan D, Tournois P (2002) Theory and performance of the acousto optic programmable dispersive filter used for femtosecond laser pulse shaping. J Phys IV 12:69–75 doi:10.1051/jp4:20020098
26. Wu J, Berland K (2007) Fluorescence intensity is a poor predictor of saturation effects in two-photon microscopy: Artifacts in fluorescence correlation spectroscopy. Microsc Res Tech 70:682–686 doi:10.1002/jemt.20454
27. Widengren J, Rigler R (1996) Mechanisms of photobleaching investigated by fluorescence correlation spectroscopy. Bioimaging 4:149–157
28. Siegman AE (1987) Lasers. Am J Phys 55:862 doi:10.1119/1.14984
29. Bardeen CJ, Wang Q, Shank CV (1998) Femtosecond chirped pulse excitation of vibrational wave packets in LD690 and bacteriorhodopsin. J Phys Chem A 102:2759–2766 doi:10.1021/jp980346k

30. Pearson BJ, White JL, Weinacht TC, Bucksbaum PH (2001) Coherent control using adaptive learning algorithms. Phys Rev A 63:063412 doi:10.1103/PhysRevA.63.063412
31. Tkaczyk ER, Mignot A, Ye JY, Majoros I, Baker JR, Norris TB (2006) Increasing two-photon fluorescence signals by coherent control. Proceedings of the SPIE 6089:165–174
32. Laarmann T, Shchatsinin I, Singh P, Zhavoronkov N, Gerhards M, Schulz CP, Hertel IV (2007) Coherent control of bond breaking in amino acid complexes with tailored femtosecond pulses. J Chem Phys 127(20):201101 doi:10.1063/1.2806029
33. Trebino R, Delong K, Fittinghoff D, Sweetser J, Krumbugel M, Richman B, Kane D (1997) Measuring ultrashort laser pulses in the time-frequency domain using frequency-resolved optical gating. Rev Sci Instrum 68:3277–3295 doi:10.1063/1.1148286
34. Weiner A (1983) Effect of group velocity mismatch on the measurement of ultrashort optical pulses via second harmonic generation. IEEE J Quantum Electron 19:1276–1283 doi:10.1109/JQE.1983.1072036
35. Ogilvie J, Kubarych K, Alexandrou A, Joffre M (2005) Fourier transform measurement of two-photon excitation spectra: applications to microscopy and optimal control. Opt Lett 30:911–913 doi:10.1364/OL.30.000911
36. Bellini M, Bartoli A, Hänsch TW (1997) Two-photon Fourier spectroscopy with femtosecond light pulses. Opt Lett 22:540–542 doi:10.1364/OL.22.000540
37. Naganuma K, Mogi K, Yamada H (1989) General method for ultrashort light pulse chirp measurement. IEEE J Quantum Electron 25:1225–1233 doi:10.1109/3.29252
38. Trebino R (2002) Frequency-resolved optical gating: The measurement of ultrashort laser pulses. Springer, New York
39. Makarov N, Drobizhev M, Rebane A (2008) Two-photon absorption standards in the 550–1,600 nm excitation wavelength range. Opt Express 16:4029–4047 doi:10.1364/OE.16.004029
40. So P, Dong C, Masters B, Berland K (2000) Two-photon excitation fluorescence microscopy. Annu Rev Biomed Eng 2:399–429 doi:10.1146/annurev.bioeng.2.1.399
41. Xu C, Zipfel W, Shear J, Williams R, Webb W (1996) Multiphoton fluorescence excitation: New spectral windows for biological nonlinear microscopy. Proc Natl Acad Sci USA 93:10763–10768 doi:10.1073/pnas.93.20.10763
42. Denk W, Svoboda K (1997) Photon upmanship: why multiphoton imaging is more than a gimmick. Neuron 18:351–357 doi:10.1016/S0896-6273(00)81237-4
43. Tkaczyk ER, Tkaczyk AH, Mauring K, Ye JY, Baker JR, Norris TB (2008) Quantitative differentiation of dyes with overlapping one-photon spectra by femtosecond pulse shaping. submitted to Chem Phys Lett
44. Bestvater F, Spiess E, Stobrawa G, Hacker M, Feurer T, Porwol T, Berchner-Pfannschmidt U, Wotzlaw C, Acker H (2002) Two-photon fluorescence absorption and emission spectra of dyes relevant for cell imaging. J Microsc 208:108–115 doi:10.1046/j.1365-2818.2002.01074.x
45. Brixner T, Damrauer NH, Kiefer B, Gerber G (2003) Liquid-phase adaptive femtosecond quantum control: Removing intrinsic intensity dependencies. J Chem Phys 118:3692–3701 doi:10.1063/1.1538239
46. Brixner T, Kiefer B, Gerber G (2001) Problem complexity in femtosecond quantum control. Chem Phys 267:241–246 doi:10.1016/S0301-0104(01)00223-3
47. Prokhorenko VI, Nagy AM, Miller RJD (2005) Coherent control of the population transfer in complex solvated molecules at weak excitation. An experimental study. J Chem Phys 122(18):184502 doi:10.1063/1.1886750
48. Pastirk I, Dela Cruz J, Walowicz K, Lozovoy V, Dantus M (2003) Selective two-photon microscopy with shaped femtosecond pulses. Opt Express 11:1695–1701
49. Delacruz JM, Pastirk I, Lozovoy VV, Walowicz KA, Dantus M (2004) Multiphoton intrapulse interference 3: probing microscopic chemical environments. J Phys Chem A 108:53–58 doi:10.1021/jp036150o
50. Du H, Fuh R-CA, Li J, Corkan LA, Lindsey JS (1998) PhotochemCAD: A computer-aided design and research tool in photochemistry. Photochem Photobiol 68:141–142
51. Invitrogen (2008) http://probes.invitrogen.com/servlets/spectra. Invitrogen Website
52. Tkaczyk ER, Mauring K, Tkaczyk AH, Krasnenko V, Ye JY, Baker JR, Norris TB (2008) Control of the blue fluorescent protein with advanced evolutionary pulse shaping. Biochem Biophys Research Commun 376(4):733–737